Tailoring the Electric Field Response of Porous BaTiO3 Ceramics Fabricated via a Sucrose-Assisted Process

Muhammad Wasim , Evangelos Kordatos , Antonio Feteira * , Iasmi Sterianou

Posted Date: 15 June 2026

doi: 10.20944/preprints202606.1124.v1

Keywords: BaTiO3; porous; microstructure; polarisation; strain; d_{33}^*

 doi:10.20944/preprints202606.1124.v1

Article

Tailoring the Electric Field Response of Porous $BaTiO_3$ Ceramics Fabricated via a Sucrose-Assisted Process

Muhammad Wasim, Evangelos Kordatos, Antonio Feteira * and Iasmi Sterianou

School of Engineering and Built Environment, Sheffield Hallam University, Sheffield S1 1WB, UK

* Correspondence: a.feteira@shu.ac.uk

Abstract

Porous $BaTiO_3$ (BTO) ceramics with controlled porosity were successfully fabricated using a simple and cost-effective sucrose-assisted route. Porosity was introduced by incorporating 10–50 vol% sucrose as a pore-forming agent, followed by sintering at 1350 °C for 2 h. The use of sucrose as an effective pore-forming agent is corroborated by the systematic reduction in bulk density from ~5.92 to ~4.1 $g.cm^{-3}$. X-ray diffraction and Raman spectroscopy analysis revealed the retention of the tetragonal phase across all samples, indicating that the introduction of porosity does not alter either the average crystal or local structure. Microstructural analysis demonstrated well-developed grains with heterogeneously distributed and interconnected porosity upon sucrose addition, while maintaining good grain connectivity. Electrical characterisation showed a gradual decrease in maximum polarisation (P_{max}) from ~21 $\mu C.cm^{-2}$ for dense BTO to ~12 $\mu C.cm^{-2}$ for 50 vol% sucrose samples. Despite increased porosity, the electric field-induced strain response exhibited only a marginal reduction (~0.137% to 0.10%), indicating preserved electromechanical functionality with enhanced large-signal piezoelectric coefficient d^*_{33} ~468 $pm.V^{-1}$ for the 20 vol% sucrose sample, whereas the 10 vol% counterpart shows the largest ε_{RT} ~1150 with tan δ = 0.005. These results demonstrate that sucrose-assisted fabrication enables effective porosity engineering in BTO without compromising its ferroelectric nature, offering a promising approach for the development of porous ferroelectric ceramics with tunable electromechanical properties.

Keywords: $BaTiO_3$; porous; microstructure; polarisation; strain; d^*_{33}

1. Introduction

Ferroelectric ceramics have attracted considerable attention due to their excellent dielectric and electromechanical properties, making them suitable for applications in sensors, actuators and energy-related devices [1,2]. Among these materials, barium titanate (BTO) remains one of the most widely studied ferroelectrics, with a stable tetragonal phase at room temperature [3]. However, with the increasing demand for lightweight [4,5] and energy-efficient devices, there is a growing need to tailor the structural design of such materials without significantly compromising their functional performance [6,7].

The introduction of controlled porosity has emerged as an effective strategy to reduce acoustic impedance and enhancing the piezoelectric voltage coefficient (g_{33}) and energy harvesting. Hence, porous ferroelectrics are also particularly attractive for sensor applications requiring reduced weight and enhanced mechanical compliance [8,9] but also in piezo-catalysis. Often the incorporation of porosity is accompanied by a deterioration in electrical properties, primarily due to the reduction in active ferroelectric volume and the development of local electric field inhomogeneities by pores [10]. As a result, achieving a balance between reduced density and preserved electromechanical performance remains a significant challenge.

 doi:10.20944/preprints202606.1124.v1

Various processing approaches have been developed to introduce controlled porosity in ceramic systems, including polymer foam replication, sacrificial templating, aerogel-based processing, freeze casting, and tape casting techniques [6,11–15]. While these methods enable control over pore architecture, they are often associated with increased processing complexity, limited scalability or restricted porosity ranges and most importantly high processing costs. In addition, much of the existing work has focused on complex or doped systems [10,16], whereas comparatively fewer studies have addressed porosity engineering in pure BTO while maintaining its intrinsic ferroelectric characteristics [17–21].

In this context, the use of sacrificial pore-forming agents such as sucrose offers a simple, cost-effective and scalable route for introducing controlled porosity [10]. Sucrose undergoes non-hazardous thermal decomposition and can generate well-distributed pore structures without introducing secondary phases. Although such approaches have been explored in related ferroelectric systems, a systematic understanding of how porosity influences the electromechanical response of undoped BTO, particularly in terms of maintaining or enhancing strain and large-signal piezoelectric behaviour remains limited.

In the present work, porous BTO ceramics with controlled porosity were fabricated using a sucrose-assisted route by conventional sintering. The study focuses on the relationship between porosity, microstructure and functional properties, with particular emphasis on polarisation, strain, large-signal piezoelectric response (d^*_{33}) and dielectric permittivity. Structural analysis confirms that the introduction of porosity does not alter the crystal structure, while the electromechanical response is maintained and, in some cases, slightly enhanced at moderate porosity levels. These findings highlight the potential of porosity engineering as an effective strategy for developing lightweight ferroelectric ceramics with stable electromechanical performance.

2. Materials and Methods

Porous $BaTiO_3$ (BTO) ceramics were prepared using BTO powder (200 nm). Controlled porosity was introduced by mixing the BTO powder with sucrose as a sacrificial pore-forming agent at volume fractions of 10, 20, 30, 40, and 50 vol%. The powders were homogenised using a conventional mortar and pestle with isopropanol as the mixing medium, followed by drying to remove the solvent. The mixed powders were uniaxially pressed into disc-shaped pellets with a diameter of 10 mm and a thickness of approximately 1.5 mm. The green pellets were sintered at 1350 °C for 2h in air using a heating and cooling rate of 5 °C.min^{-1} in covered crucible to obtain porous BTO ceramics. The radial shrinkage and bulk density were determined by measuring the diameter and thickness of the sintered pellets, and the weight was measured using a digital scale. Phase purity and crystal structure of the sintered samples were examined using X-ray diffraction (XRD) with Co Kα radiation (λ = 1.789 Å) in the 2θ range of 10°–90°. Rietveld refinement of the XRD data was performed using HighScore to determine crystal structure and lattice parameters. Raman spectroscopy was performed using a Thermo DXR2 Raman microscope equipped with a 532 nm laser to further examine their local structure. Microstructural analysis was carried out using tungsten filament, scanning electron microscope (FE-SEM, Quanta 650, FEI, Czech Republic).

For electrical measurements, platinum electrodes were applied to both faces of the polished pellets and heat-treated at 600 °C for 30 min to ensure good electrical contacts. Polarisation–electric field (P–E) hysteresis loops, strain–electric field (S–E) loops, and large-signal piezoelectric response (d^*_{33}) were measured at room temperature using an aixACCT TF-2000 ferroelectric tester operated at a frequency of 1 Hz. Dielectric permittivity was measured at room temperature at a frequency of 100 kHz using an HP 4284A Precision LCR Meter (Agilent Technologies, USA).

 doi:10.20944/preprints202606.1124.v1

3. Results and Discussion

3.1. Bulk Density and Porosity

The bulk density and corresponding porosity of BTO ceramics as a function of sucrose content are presented in Figure 1(a, b), respectively. The BTO sample exhibits a high bulk density of ~5.92 g.cm^{-3}, indicating effective densification under the applied sintering conditions, considering that the theoretical density of BTO is 6.02 g.cm^{-3}. Upon the introduction of sucrose, the reduction in density is not strictly linear at low concentrations. In particular, the sample with 10 vol% sucrose shows only a marginal decrease in bulk density, which may be attributed to the partial role of sucrose in enhancing particle packing or acting as a temporary binder during compaction, as reported in previous studies [22]. Nevertheless, the decomposition of sucrose during heat treatment still leads to the formation of a limited amount of porosity, resulting in a slightly lower density compared to BTO.

With further increase in sucrose content (20–50 vol%), a clear decreasing trend in bulk density is observed, reaching ~4.1 g.cm^{-3} for the 50 vol% sample. This behaviour reflects the dominant effect of pore formation at higher pore-former concentrations, where the increasing volume fraction of decomposed sucrose leads to a more significant reduction in the effective ceramic density. However, as the sucrose content increased to 50 vol%, a significant decrease in density (~30%) was recorded, confirming the effective formation of porosity within the BTO matrix.

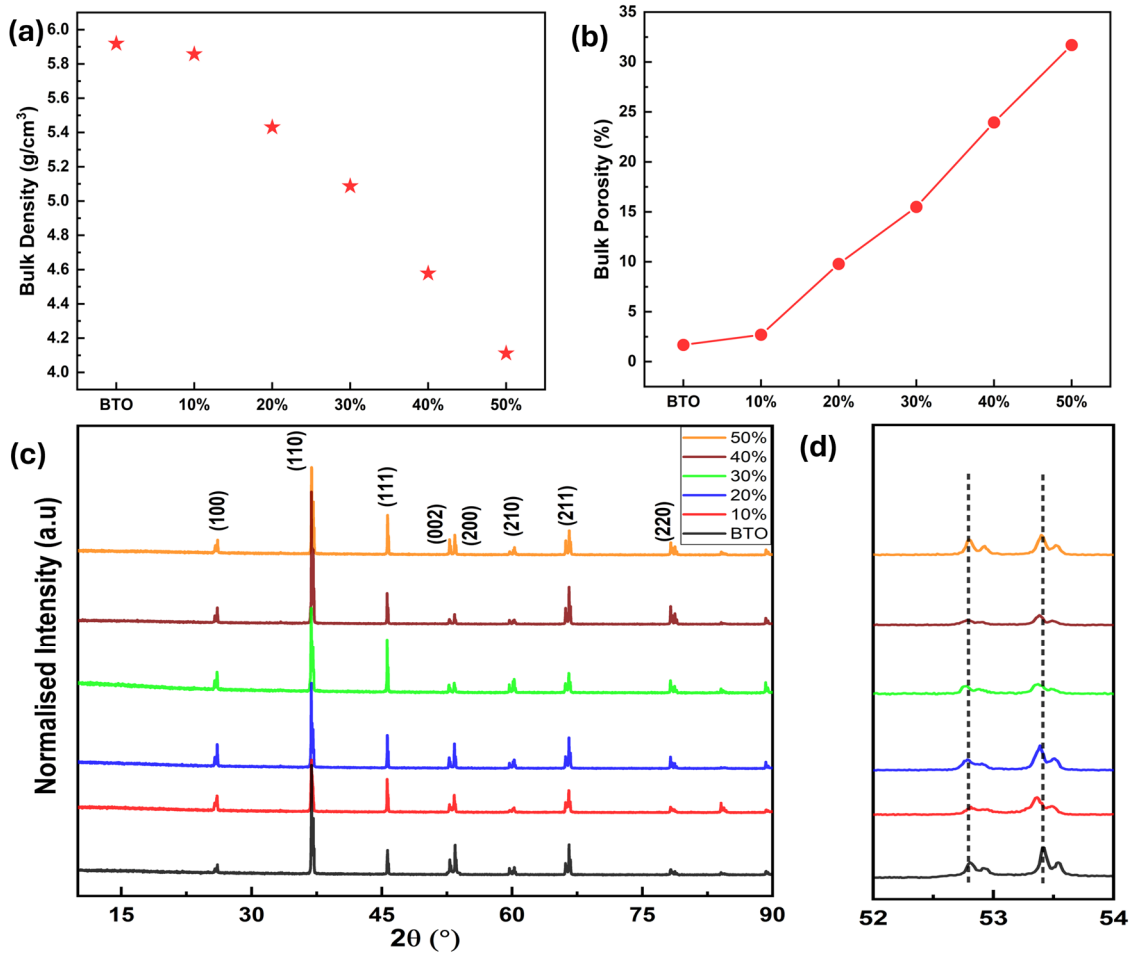

Figure 1. (a) Bulk density, (b) Bulk porosity, (c,d) XRD data and zoom region of 52 to 54° 2θ shows the 002 and 200 peaks, respectively for BTO and BTO + Sucrose ceramics sintered at 1350 °C.

 doi:10.20944/preprints202606.1124.v1

The corresponding porosity values, calculated using Equation (1), increased from ~1.7% for dense BTO to ~31.7% for the highest sucrose content. The porosity (P) was determined using equation 1.

$$P = \left(1 - \frac{\rho_{BD}}{\rho_{TD}}\right) * 100 \quad (1)$$

where ρ_{TD} is the theoretical density of BTO (6.02 g.cm^{-3}) and ρ_{BD} is the measured bulk density obtained using the geometric method.

It is important to note that the measured porosity does not show a direct linear relationship with the initial sucrose volume fraction. This deviation can be attributed to the combined effects of pore formation and sintering-induced densification. During heat treatment, sucrose undergoes thermal decomposition, generating voids that act as pore former. However, at elevated temperatures, partial densification of the ceramic matrix, along with shrinkage and coalescence of pores, reduces the final pore volume relative to the initial sucrose content [4]. As a result, the effective porosity remains lower than the nominal pore-former fraction across all compositions.

3.2. Phase Purity and Crystal Structure

The X-ray diffraction (XRD) patterns of BTO ceramics with varying sucrose content (Figure 1(c,d)) show a well-defined tetragonal phase with space group P4mm [23,24], consistent with the standard reference pattern (ICDD #01-085-9527). The clear splitting of the {002}/{200} reflections confirm the presence of the ferroelectric tetragonal structure at room temperature [23]. No additional diffraction peaks corresponding to secondary phases are observed for any sample (0–50 vol% sucrose), indicating that the phase purity is preserved and the tetragonal structure is retained despite the introduction of porosity.

Lattice parameter refinements were performed to further examine possible structural variations, and those are summarised in Table 1. The results show that the lattice parameters and unit cell volume exhibit only very minor variations across the compositional range. The tetragonality (c/a ratio) remains close to that of BTO for all samples, with only a slight reduction observed for the 10 vol% composition. Across the full series, the tetragonality (c/a) is 1.0103 ± 0.0002. Considering the small magnitude of these variations and the associated refinement uncertainty, no systematic trend in lattice distortion is evident.

Table 1. Refined lattice parameters, c/a ratio, unit cell volume and goodness-of-fit (GOF) of all compositions.

Composition	Space Group	Lattice Parameters		c/a ratio	Volume (Å)	GOF
		a, b (Å)	c (Å)			
BTO	P4mm	3.994(9)	4.036(1)	1.0104	64.38(2)	1.87
10%	P4mm	3.994(3)	4.035(4)	1.0102	64.36(3)	2.55
20%	P4mm	3.994(6)	4.036(7)	1.0104	64.37(1)	2.10
30%	P4mm	3.994(8)	4.036(9)	1.0105	64.38(2)	1.83
40%	P4mm	3.994(6)	4.036(7)	1.0105	64.38(2)	2.22
50%	P4mm	3.994(6)	4.036(6)	1.0105	64.38(1)	1.72

Overall, these results indicate that the introduction of porosity via the sucrose-assisted route does not induce any detectable phase transformation or significant modification of the crystal structure. Therefore, the changes observed in the dielectric and electromechanical properties are primarily attributed to microstructural effects associated with porosity rather than alterations in the intrinsic crystal structure.

3.3. Raman Spectroscopy Analysis

Raman spectroscopy was employed to further examine the local structure of BTO ceramics with varying sucrose content, and the corresponding spectra are presented in Figure 2(a–c). The dense

 doi:10.20944/preprints202606.1124.v1

BTO sample exhibits the characteristic Raman-active modes of the tetragonal phase, confirming the presence of long-range ferroelectric order [25,26]. No additional modes associated with secondary phases are observed across all compositions, which is consistent with the XRD results and indicates that the incorporation of porosity does not alter the phase purity of the material. The prominent Raman modes observed at approximately ~305 cm^{-1} and ~720 cm^{-1} correspond to the $E(TO_2)$ and $A_1(LO_2)$ vibrations, respectively, which are well-known signatures of tetragonal BTO. The $E(TO_2)$ mode is commonly associated with the ferroelectric nature of BTO and is often considered a fingerprint of spontaneous polarisation, while the $A_1(TO_2)$ mode Ti-O is sensitive to local lattice vibration and internal strain [27]. A closer inspection of the spectra in the regions 225–325 cm^{-1} and 450–600 cm^{-1}, as shown in Figure 2(b, c) respectively, reveals there are not even minor variations in mode frequency with increasing sucrose content.

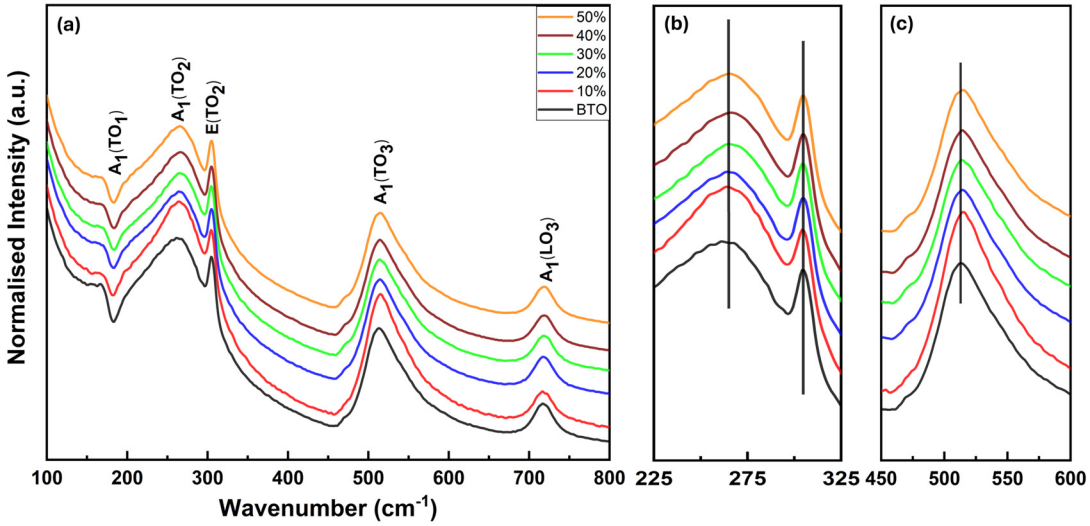

Figure 2. (a) Raman spectra BTO and BTO + Sucrose ceramics sintered at 1350 ºC and (b, c) blow-up of region of 225 to 325 and 450 to 600 cm^{-1}, respectively.

Overall, the retention of all characteristic Raman modes, along with the absence of any additional features, confirms that the local structure of BTO is preserved without stresses acting on grains of ceramics with different levels of porosity. These results are in good agreement with the XRD analysis, demonstrating that the sucrose-assisted process to create controlled porosity does neither affect the crystallographic structure nor creates local lattice distortions [28].

3.4. Microstructure Analysis

The surface morphology of BTO ceramics with varying sucrose content is shown in Figure 3(a–f). The BTO sample (Figure 3a) exhibits well-defined, polyhedral grains with an average grain size of ~75–100 μm. The grains are closely packed with well-developed grain boundaries, indicating effective densification and minimal porosity, which is consistent with the bulk density. Furthermore, energy-dispersive X-ray (EDX) analysis (Supplementary Figure S1) confirms as expected that the elemental composition remains unchanged with the introduction of porosity, indicating that the sucrose-assisted process does not alter the chemical stoichiometry of the BTO ceramics.

With the introduction of sucrose (Figure 3b–f), a gradual evolution in microstructure is observed, characterised by the progressive formation and growth of pores. At lower concentrations, pores appear as isolated features within grains and along grain boundaries as shown in Figure 3b,c, while increasing sucrose content leads to a higher pore density and enlargement of pore size. At higher concentrations, the pores become more irregular in shape and more non-uniformly distributed, resulting in the formation of a well-developed porous network across the surface shown in Supplementary Figure S2.

 doi:10.20944/preprints202606.1124.v1

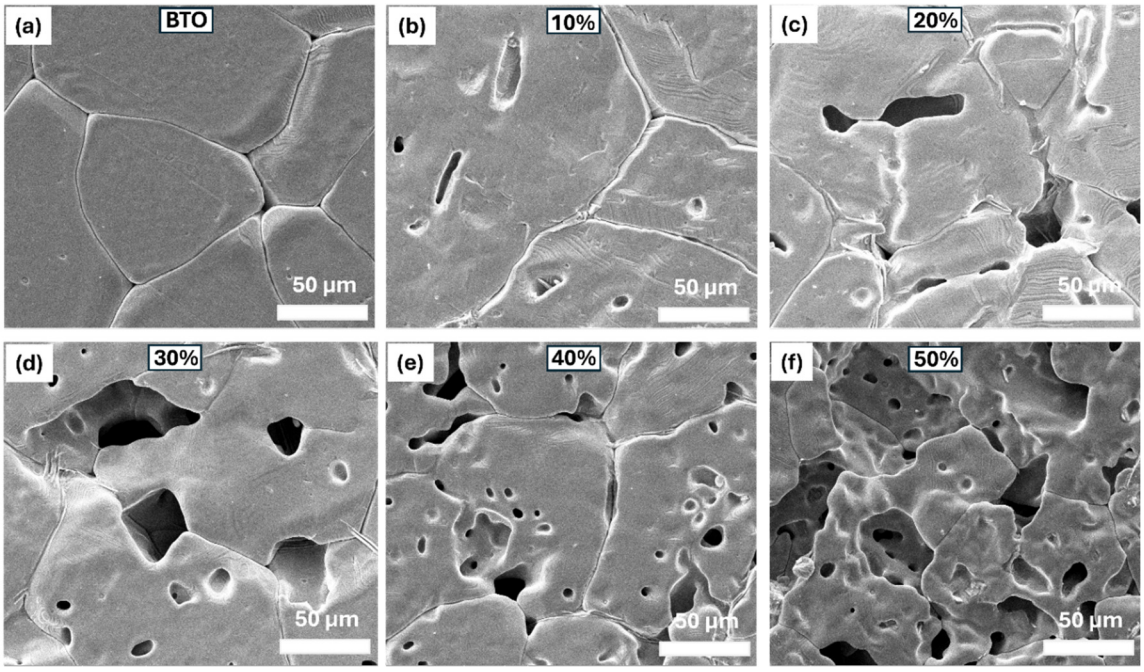

Figure 3. Microstructures of BTO and BTO + Sucrose ceramics sintered at 1350 ºC for 2 h.

To further examine the pore connectivity, cross-sectional SEM images are presented in Figure 4 at different magnifications (from ~1 mm to ~0.05 mm scale). The cross-sectional analysis reveals that the pores are not limited to the surface but are distributed throughout the bulk of the material. At higher magnifications, a clear interconnected pore network can be observed, confirming that the porosity extends across the entire sample. This interconnected structure suggests the formation of continuous pathways within the ceramic matrix, which is consistent with the observed reduction in density and supports the effectiveness of the sucrose-assisted processing route. Importantly, despite the significant increase in porosity, the grains remain well connected across all compositions. This indicates that the ceramic matrix maintains structural continuity even at high porosity levels, which is essential for preserving functional pathways for polarisation and strain response.

3.5. High Field Electrical Measurements

The bipolar polarisation–electric field (P–E), strain–electric field (S–E) and switching current responses of BTO ceramics with varying porosity were measured at room temperature under an applied field of 30 kV.cm^{-1} and a frequency of 1 Hz, as shown in Figure 5(a–c). The dense BTO sample exhibits a well-defined ferroelectric hysteresis loop with a maximum polarisation (P_{max}) of ~21 µC.cm^{-2}, remanent polarisation (Pr) of ~13 µC.cm^{-2}, and a coercive field (Ec) of ~5 kV.cm^{-1}, consistent with typical ferroelectric behaviour [29].

The evolution of polarisation with increasing porosity does not follow a strictly linear trend. While an overall decrease in P_{max} is observed with increasing porosity, the rate of reduction varies across compositions. In particular, the difference in P_{max} between intermediate porosity levels (20–30 vol% nominal) is relatively small, and a similar behaviour is observed between higher porosity samples (40–50 vol% nominal). This indicates that the influence of porosity on polarisation is not proportional to the nominal pore volume fraction. Such behaviour can be attributed to the inhomogeneous distribution of pores and the resulting local electric field variations within the ceramic matrix [28]. At low to moderate porosity, the ferroelectric regions remain sufficiently connected, allowing effective polarisation switching, and thus only a gradual reduction in P_{max} is observed [6,10]. As the porosity increases further, the reduction becomes more pronounced; however, beyond a certain level, the change tends to stabilise due to the already reduced active ferroelectric

 doi:10.20944/preprints202606.1124.v1

volume. Therefore, the observed behaviour reflects a progressive but non-linear dependence of polarisation on porosity.

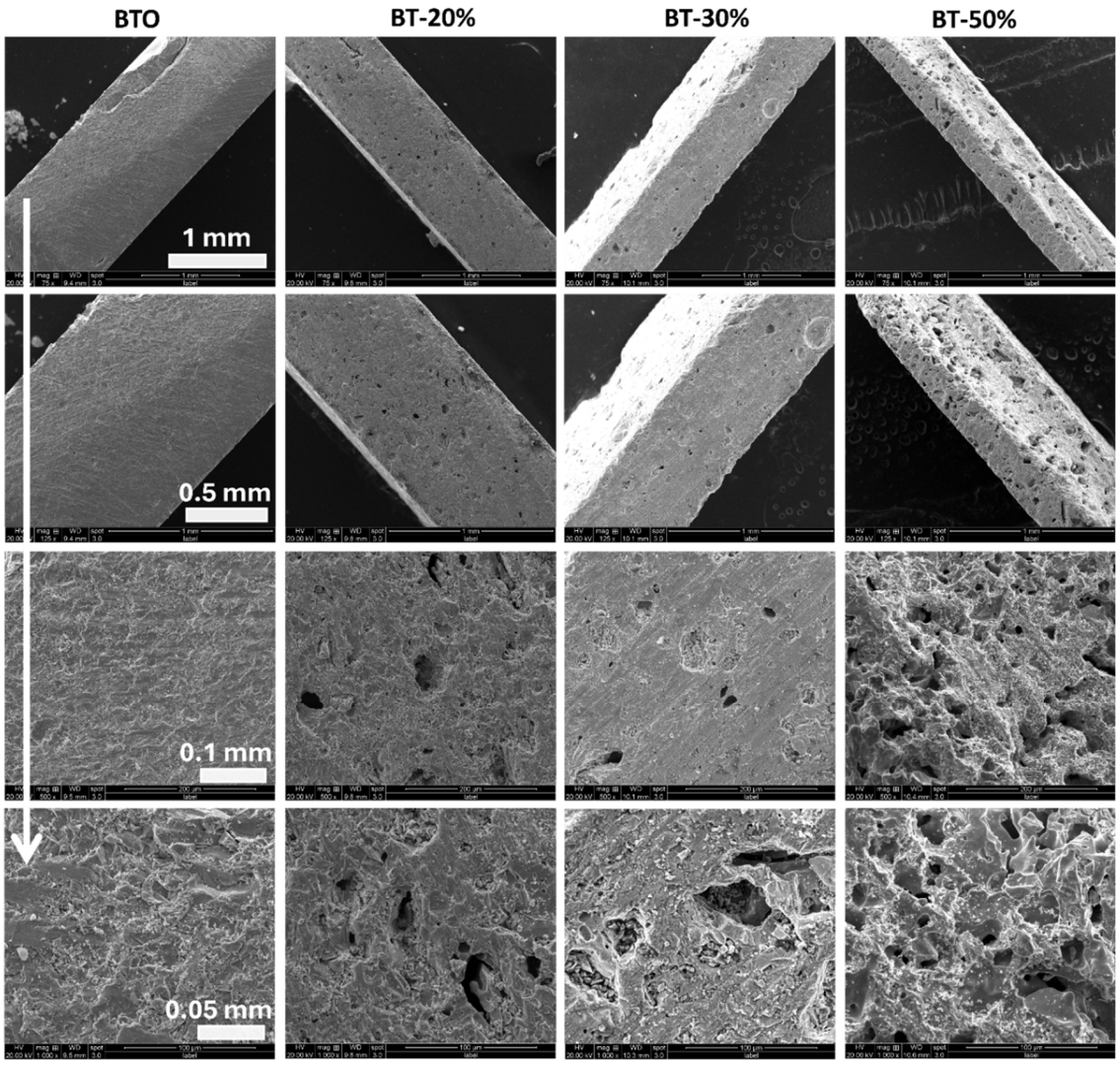

Figure 4. Microstructure of cross-section of BTO and BTO + Sucrose (20, 30 and 50 vol%) ceramics sintered at 1350 ºC for 2 h, at different magnifications.

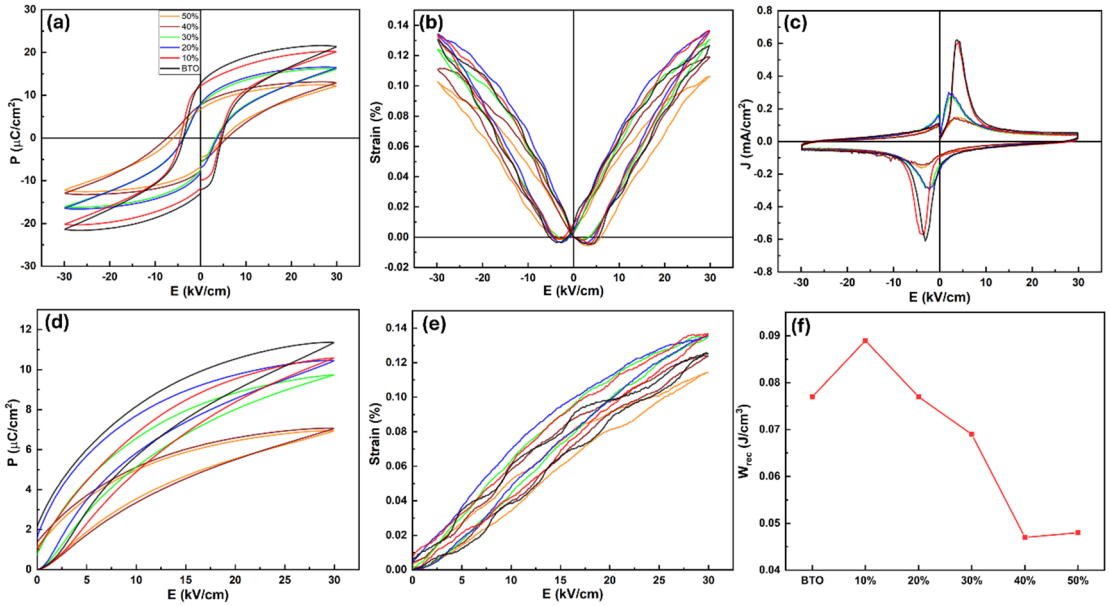

 doi:10.20944/preprints202606.1124.v1

Figure 5. (a-c) Bipolar electrical polarisation, strain (%) and current loops at 30 kV.cm^{-1}, (d-f) Unipolar polarisation, strain (%) and W_{rec} (%) at 30 kV.cm^{-1}, respectively, for BTO and BTO + Sucrose ceramics sintered at 1350 ºC for 2h.

In contrast to the polarisation behaviour, the strain response exhibits a different trend. The dense BTO sample shows a maximum strain of ~0.125%, while the samples with 10–20 vol% nominal porosity display a slight enhancement, reaching ~0.137% as shown in Figure 5e. This behaviour can be attributed to reduced mechanical constraint within the porous structure, which facilitates domain switching under the applied electric field. At higher porosity levels (30–50 vol% nominal), the strain shows a gradual decrease; however, it remains relatively stable (~0.12–0.10%) compared to the corresponding reduction in polarisation. This indicates that the electromechanical response is less sensitive to porosity than the polarisation behaviour. It suggests that the porous structure facilitates deformation despite the reduction in active material.

The current density (J–E) loops (Figure 5c) further support the observed switching behaviour. The dense and low-porosity samples exhibit relatively sharp current peaks near the coercive field, corresponding to domain switching. With increasing porosity, the peaks become broader and less pronounced, indicating wider distribution of local electric fields within the porous structure and distribution of domain switching events.

The unipolar P–E and S–E responses (Figure 5d,e) show progressively slimmer hysteresis with increasing porosity, reflecting reduced hysteresis losses. The recoverable energy density (W_{rec}), calculated from the unipolar loops (Figure 5f), shows a slight enhancement for the 10 vol% sample (~0.09 J.cm^{-3}) compared to dense BTO, followed by a gradual decrease at higher porosity levels. This behaviour is consistent with the reduction in polarisation and the change in loop shape. However, the overall magnitude of W_{rec} remains relatively low, and thus energy storage is not the primary focus of the present study.

3.6. Relative Permittivity and Large-Signal Piezoelectric Coefficient, d^*_{33}

The dielectric properties measured at room temperature and 100 kHz are presented in Figure 6a. The dense BTO sample exhibits a relative permittivity of ~1010 with a dielectric loss of ~0.019, which is consistent with typical values reported for BTO ceramics [3]. With the introduction of 10 vol% nominal porosity, the permittivity increases to ~1175, accompanied by a significant reduction in dielectric loss (~0.005). This improvement suggests that a small degree of porosity can enhance dielectric response while maintaining low energy dissipation [28,30]. At 20 vol%, the permittivity remains relatively high (~1075) with low loss, whereas further increases in porosity (30–50 vol% nominal) lead to a gradual reduction in permittivity (~650 at 50 vol%), primarily due to the decreasing volume fraction of the active BTO content [6].

The large-signal piezoelectric coefficient (d^*_{33}), derived from the unipolar strain–electric field response at 30 kV.cm^{-1} and 1 Hz, is shown in Figure 6(b). The dense BTO sample exhibits a d_{33} of ~404 pm.V^{-1}. With increasing porosity, d^*_{33} increases to ~454 pm.V^{-1} (10 vol%) and reaches a maximum of ~468 pm·V^{-1} at 20 vol%, while remaining high (~462 pm.V^{-1}) at 30 vol%. This enhancement at moderate porosity is consistent with the observed strain behaviour and can be attributed to reduced mechanical constraint within the porous structure, allowing more effective electromechanical deformation under an applied field. At higher porosity levels, d^*_{33} decreases to ~422 and ~378 pm.V^{-1}, respectively, due to the reduced active material volume and increased structural discontinuity.

 doi:10.20944/preprints202606.1124.v1

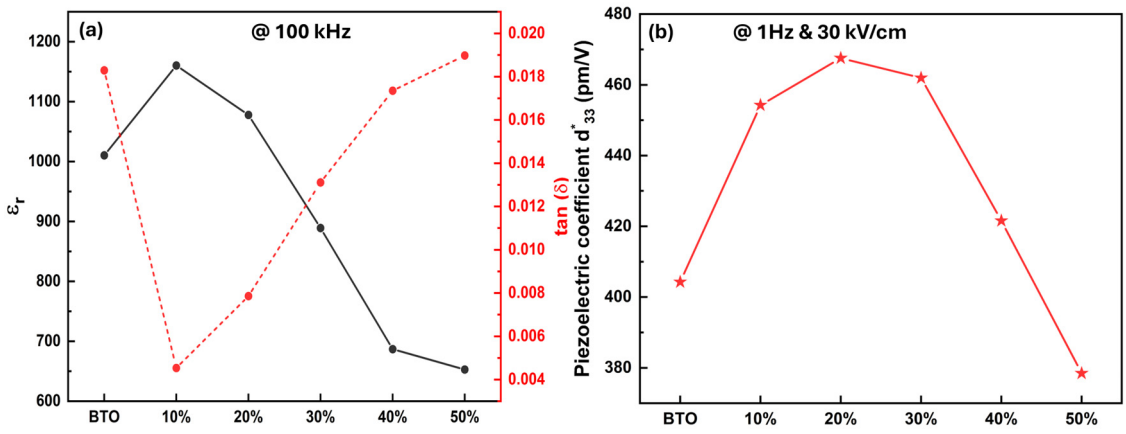

Figure 6. (a) Relative permittivity and loss at room temperature and (b) piezoelectric coefficient, d^*_{33}, at room temperature and high field 30 kV.cm^{-1} for BTO and BTO + Sucrose ceramics sintered at 1350 ºC for 2h.

Overall, the electrical results demonstrate that while polarisation decreases with increasing porosity, the strain response and large-signal piezoelectric behaviour are preserved and even enhanced at moderate porosity levels. This highlights the potential of porosity engineering as an effective approach to achieve lightweight BTO ceramics with stable electromechanical performance.

5. Conclusions

Porous barium titanate (BTO) ceramics were successfully fabricated using a simple sucrose-assisted route, enabling regulated porosity in the range of ~2% to ~32%. Crystal structure analysis confirmed that the tetragonal P4mm phase is retained across all compositions, indicating that the introduction of porosity does not significantly affect the crystal structure. The incorporation of porosity leads to a systematic reduction in polarisation due to the decrease in effective ferroelectric volume and the presence of local electric field inhomogeneities. In contrast, the strain response and d^*_{33} are preserved and even enhanced at moderate porosity levels (2–10%), reaching a maximum d^*_{33} of ~468 pm.V^{-1}. This behaviour is attributed to reduced mechanical constraint within the porous structure, which facilitates electromechanical deformation under an applied electric field. Dielectric measurements further show that low levels of porosity (2–10%) can improve permittivity while maintaining low dielectric loss, whereas higher porosity leads to a gradual decline due to the increasing contribution of the pore phase. Overall, these results demonstrate that controlled porosity can effectively tailor the structure–property relationships in BTO without compromising its ferroelectric phase stability. This study highlights porosity engineering as a viable strategy for developing lightweight ferroelectric ceramics with stable electromechanical performance, particularly in applications where reduced density and reliable strain response are required.

Supplementary Materials: The following supporting information can be downloaded at the website of this paper posted on Preprints.org.

Author Contributions: M.W; Writing–original draft, Investigation, Methodology, Data curation, Formal Analysis, Conceptualisation. **E.K;** Supervision, Validation. **I.S** and **A.F;** Writing—review & editing, Supervision, Resources, Validation, Conceptualisation, Investigation.

Funding: The financial support provided through the PhD Graduate Teaching Assistantship (GTA) scholarship scheme at Sheffield Hallam University, UK.

Data Availability Statement: For the purpose of open access, the author has applied a Creative Commons Attribution (CC BY) licence to any Author Accepted Manuscript arising from this submission.

 doi:10.20944/preprints202606.1124.v1

Acknowledgments: The author gratefully acknowledges the financial support provided through the PhD Graduate Teaching Assistantship (GTA) scholarship scheme at Sheffield Hallam University, UK.

Conflicts of Interest: The authors declare that they have no known competing financial interests or personal relationships that could have appeared to influence the work reported in this paper.

Abbreviations

The following abbreviations are used in this manuscript:

BTO	Barium Titanate/$BaTiO_3$
XRD	X-ray diffraction
SEM	Scanning electron microscopy
EDX	Energy-dispersive X-ray spectroscopy
P-E	Polarisation–electric field
S-E	Strain–electric field
J-E	Current density–electric field
P_{max}	Maximum Polarisation
P_r	Remanent polarization
E_c	Coercive Field
W_{rec}	Recoverable energy density
d_{33}^*	Large-signal piezoelectric coefficient
ICDD	International Centre for Diffraction Data
GOF	Goodness of fit
LCR	Inductance–capacitance–resistance meter

References

1. Zubairi, H., Lu, Z., Zhu, Y., Reaney, I. M. & Wang, G. Current development, optimisation strategies and future perspectives for lead-free dielectric ceramics in high field and high energy density capacitors. *Chemical Society Reviews*. **2024**, *53*, 10761-10790.
2. Wang, G. et al. Electroceramics for High-Energy Density Capacitors: Current Status and Future Perspectives. *Chemical Reviews*. **2021**, *121*, 6124–6172.
3. Sada, T. et al. High permittivity $BaTiO_3$ and $BaTiO_3$-polymer nanocomposites enabled by cold sintering with a new transient chemistry: Ba(OH)2·8H_2O. *J. Eur. Ceram. Soc.* **2021,** *41*, 409–417.
4. Chen, Y., Wang, N., Ola, O., Xia, Y. & Zhu, Y. Porous ceramics: Light in weight but heavy in energy and environment technologies. *Materials Science and Engineering: R: Reports*. **2021**, *143*, 100589.
5. Hammel, E. C., Ighodaro, O. L. R. & Okoli, O. I. Processing and properties of advanced porous ceramics: An application based review. *Ceram. Int.* **2014**, *40*, 15351–15370.
6. Zhang, Y. et al. Enhanced pyroelectric and piezoelectric properties of PZT with aligned porosity for energy harvesting applications. *J. Mater. Chem. A*. **2017**, *5*, 6569–6580.
7. Roscow, J., Zhang, Y., Taylor, J. & Bowen, C. R. Porous ferroelectrics for energy harvesting applications. *European Physical Journal: Special Topics*. **2015**, *224*, 2949–2966.
8. Bowen, C. R. & Kara, H. Pore Anisotropy in 3-3 Piezoelectric Composites. *Materials Chemistry and Physics*. **2002**, *75*, 45-49.
9. Bowen, C. R., Perry, A., Lewis, A. C. F. & Kara, H. Processing and properties of porous piezoelectric materials with high hydrostatic figures of merit. *J. Eur. Ceram. Soc.* **2004**, *24*, 541–545.
10. Abhinay, S., Dixit, P. & Mazumder, R. Effect of pore former sucrose on microstructure and electrical properties of porous BZT-0.5BCT ceramics. *Ferroelectrics*. **2020**, *557*, 18–27.
11. Creedon, M. J. & Schulze, W. A. Axially distorted 3–3 piezoelectric composites for hydrophone applications. *Ferroelectrics*. **1994**, *153*, 333–339.
12. Newnham, R. E., Skinner, D. P. & Cross, L. E. Connectivity and piezoelectric-pyroelectric composites. *Mater. Res. Bull.* **1978**, *13*, 525–536.

 doi:10.20944/preprints202606.1124.v1

13. Geis, S., Fricke, J. & Löbmann, P. Electrical properties of PZT aerogels. *J. Eur. Ceram. Soc.* **2002**, *22*, 1155–1161.
14. Craciun, F., Galassi, C., Roncari, E., Filippi, A. & Guidarelli, G. Electro-elastic properties of porous piezoelectric ceramics obtained by tape casting. *Ferroelectrics.* **1998**, *205*, 49–67.
15. Rittenmyer, K., Shrout, T., Schulze, W. A. & Newnham, R. E. Piezoelectric 3–3 composites. *Ferroelectrics*. **1982**, *41*, 189–195.
16. Zeng, T., Dong, X. L., Mao, C. L., Zhou, Z. Y. & Yang, H. Effects of pore shape and porosity on the properties of porous PZT 95/5 ceramics. *J. Eur. Ceram. Soc.* **2007**, *27*, 2025–2029.
17. Hu, J., Zhang, S. & Tang, B. Three-dimensionally ordered macroporous $BaTiO_3$ framework-reinforced polymer composites with improved dielectric properties. *SN Appl. Sci.* **2021**, 3:52.
18. Jiang, Z. et al. 3D printing of porous scaffolds $BaTiO_3$ piezoelectric ceramics and regulation of their mechanical and electrical properties. *Ceram. Int.* **2022**, *48*, 6477–6487.
19. Gaur, A., Chauhan, V. S. & Vaish, R. Porous $BaTiO_3$ ceramic with enhanced piezocatalytic activity for water cleaning application. *Surfaces and Interfaces.* **2023**, *36*, 102497.
20. Lukacs, V. A. et al. Structural and functional properties of $BaTiO_3$ porous ceramics produced by using pollen as sacrificial template. *Ceram. Int*. **2020**, *46*, 523–530.
21. Roscow, J. I., Topolov, V. Y., Bowen, C. R., Taylor, J. & Panich, A. E. Understanding the peculiarities of the piezoelectric effect in macro-porous $BaTiO_3$. *Sci. Technol. Adv. Mater.* **2016**, *17*, 769–776.
22. Wiecinska, P., Zurawska, A., Falkowski, P., Jeong, D. Y. & Szafran, M. Sweet ceramics: how saccharide-based compounds have changed colloidal processing of ceramic materials. *Journal of the Korean Ceramic Society.* **2020**, *57*, 231–245.
23. Zali, N. M., Mahmood, C. S., Mohamad, S. M., Foo, C. T. & Murshidi, J. A. X-ray diffraction study of crystalline barium titanate ceramics. *AIP Conference Proceedings*. **2014**, *1584*, 160–163.
24. Biglar, M., Gromada, M., Stachowicz, F. & Trzepieciński, T. Synthesis of barium titanate piezoelectric ceramics for multilayer actuators (MLAs). *Acta Mechanica et Automatica.* **2017**, *11*, 275–279.
25. Veerapandiyan, V. K. et al. B-site vacancy induced Raman scattering in $BaTiO_3$-based ferroelectric ceramics. *J. Eur. Ceram. Soc.* **2020**, *40*, 4684–4688.
26. Deluca, M., Al-Jlaihawi, Z. G., Reichmann, K., Bell, A. M. T. & Feteira, A. Remarkable impact of low $BiYbO_3$ doping levels on the local structure and phase transitions of $BaTiO_3$. *J. Mater. Chem. A.* **2018**, *6*, 5443–5451.
27. Deluca, M., Hu, H., Popov, M. N., Spitaler, J. & Dieing, T. Advantages and developments of Raman spectroscopy for electroceramics. *Communications Materials.* **2023**, 4:78.
28. Padurariu, L. et al. Modifications of structural, dielectric and ferroelectric properties induced by porosity in $BaTiO_3$ ceramics with phase coexistence. *J. Alloys Compd.* **2021**, *889*, 161699.
29. Carroll, E. L., Killeen, J. H., Feteira, A., Dean, J. S. & Sinclair, D. C. Influence of electrode contact arrangements on Polarisation-Electric field measurements of ferroelectric ceramics: A case study of $BaTiO_3$. *Journal of Materiomics.* **2025**, *11*, 100939.
30. Jian, G. et al. Enhanced dielectric constant and energy density in a $BaTiO_3$/polymer-matrix composite sponge. *Commun. Mater*. **2020**, 1:91.